Thermoacoustic and thermoreflectance imaging of biased integrated circuits: Voltage and temperature maps

E. Hernández-Rosales,[1,2] E. Cedeño,[1,2] J. Hernandez-Wong,[2,3] J. B. Rojas-Trigos,[2] E. Marin,[2] F. C. G. Gandra,[1] and A. M. Mansanares[1,a)]
[1]*Gleb Wataghin Physics Institute, University of Campinas - Unicamp, 13083-859 Campinas, SP, Brazil*
[2]*Instituto Politécnico Nacional, Centro de Investigación en Ciencia Aplicada y Tecnología Avanzada, Legaria 694, Colonia Irrigación, CP 11500, México, DF, Mexico*
[3]*CONACYT, México, DF, México*

(Received 17 March 2016; accepted 13 July 2016; published online 25 July 2016)

In this work a combined thermoacoustic and thermoreflectance set-up was designed for imaging biased microelectronic circuits. In particular, it was used with polycrystalline silicon resistive tracks grown on a monocrystalline Si substrate mounted on a test chip. Thermoreflectance images, obtained by scanning a probe laser beam on the sample surface, clearly show the regions periodically heated by Joule effect, which are associated to the electric current distribution in the circuit. The thermoacoustic signal, detected by a pyroelectric/piezoelectric sensor beneath the chip, also discloses the Joule contribution of the whole sample. However, additional information emerges when a non-modulated laser beam is focused on the sample surface in a raster scan mode allowing imaging of the sample. The distribution of this supplementary signal is related to the voltage distribution along the circuit. *Published by AIP Publishing.* [http://dx.doi.org/10.1063/1.4959828]

Photothermal reflectance microscopy has become a very well established technique for the characterization of thermal properties of materials at the micrometer scale,[1–5] as well as for the investigation of the heat source distribution in optoelectronic and microelectronic devices in operation.[6–16] In the first case, the sample excitation is provided by an intensity modulated laser beam, which heats the sample through light absorption. The surface temperature of the sample is probed by a second non-modulated laser, whose intensity changes induced by variations in sample optical reflectance provoked by the periodical heating are detected by a photodiode coupled to a lock-in amplifier. Modulation frequencies are typically in the range of kHz to MHz to bring the characteristic thermal diffusion length to the micrometer scale.[1,2] On the other hand, in the case of operating devices, the excitation is generally done by modulated current/voltage applied to the circuit. The non-modulated probe laser beam scans the sample surface to store its thermal image. Resistive tracks,[12,15] MOSFET's,[10,11,14] solar cells,[13] and diode-lasers[6–9] were widely investigated. Joule heating is often the dominant mechanism in resistive tracks;[15] electro-reflectance and Seebeck/Peltier contributions were also reported in the devices.[11,12]

Recently, we employed a lead zirconate titanate (PZT) sensor underneath the sample to characterize liquids by scanning a pump beam along the upper surface of an absorbing material.[17,18] An extended version of this setup, combined with thermoreflectance, is used in the present work for imaging of biased microelectronic circuits. In the conventional reflectance technique, the lateral resolution (imaging) is naturally achieved by scanning the probe beam on the sample surface. The PZT sensor, on the other hand, detects the heat generated in the sample, both directly (pyroelectric effect) and through acoustic waves coupled to the temperature field (piezoelectric effect), disregarding the location of the heat source. However, it is possible to restore lateral resolution by focusing a non-modulated laser beam on the sample surface. The laser absorption creates an additional modulated signal on the PZT that is sensitive to the geometry of the sample structure (namely, distinct material layers linked to the presence of electric current/field/potential).

The resistive tracks are biased with a voltage of the form $V(t) = (V_0/2)\,[1 + \cos(\omega t)]$, with $\omega = 2\pi f$ and V_0 up to 5.0 V. The thermoacoustic signal is acquired by a pyroelectric/piezoelectric sensor, which is the active component of a commercial buzzer (BGD, Steren) connected to a lock-in amplifier. The ensemble sample-PZT (Fig. 1(a)) is placed on a motion stage with minimum step size of 0.1 μm. The conventional thermal reflectance microscopy is achieved by using an intensity modulated Ar^+ laser line as excitation (488 nm, 1.0 μm in diameter, typically few mW at the sample), and a non-modulated He-Ne laser as probe (632.8 nm, 1.2 μm in diameter, typically tens of μW at the sample), both superimposed and focused on the sample surface by an optical microscope. The reflected He-Ne beam is detected by an Si photodiode connected to a lock-in amplifier. Modulation frequencies used both in the voltage and in the excitation Ar^+ laser range between f = 25 Hz and 100 kHz. The lock-in selects the 1st or the 2nd harmonic of the signals.

The optical image of the sample consisting of polycrystalline silicon resistive tracks (6 μm and 12 μm wide, 0.42 μm thick) on monocrystalline Si substrate fabricated on a test chip is shown in Fig. 1(b). In this figure one can also see the metallic contact pads (numbers 1–4) and a metallic track (20 μm wide, 0.60 μm thick, signalized by the arrow) connecting pad number 3 to the polycrystalline silicon track. The resistive tracks are isolated from the substrate by a 0.5 μm thick SiO_2 layer. Figure 1(c) shows an electric diagram of the equivalent circuit.

a)Author to whom correspondence should be addressed. Electronic mail: manoel@ifi.unicamp.br

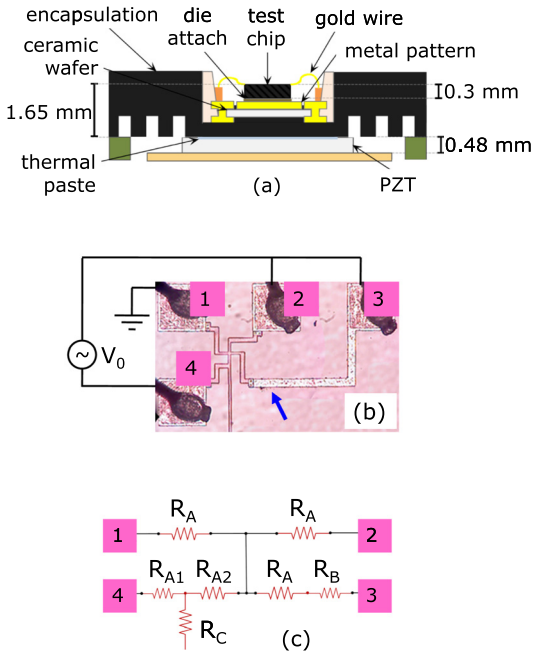

FIG. 1. (a) Cross-sectional scheme of the sample and PZT sensor. (b) Optical image of the sample showing the interconnects on an Si substrate and the applied modulated voltage. The polycrystalline silicon resistive tracks are 6 μm and 12 μm wide, and 0.42 μm thick. The metallic track is 20 μm wide and 0.60 μm thick. The resistive tracks are isolated from the substrate by a 0.5 μm thick SiO_2 layer. (c) Electric diagram of the circuit: $R_A = R_{A1} + R_{A2} = 0.32\,k\Omega$, $R_B = 0.07\,k\Omega$, $R_C = 1.86\,k\Omega$. The bottom pad (not visible) of the central line with resistance R_C is open (not connected).

Figure 2 shows the signal amplitude map of the thermoacoustic signal, detected through the PZT by using the Ar^+ laser line as excitation (conventional excitation), modulated at f = 50 Hz. The scanned area is 200 μm × 200 μm and covers the central part of the trail that includes polycrystalline silicon tracks, as shown in Fig. 1(b). It has to be observed that the signal detected by the PZT is transmitted across the sample thickness (~300 μm Si substrate followed by ~1 mm backing chip capsule), once the heat generation takes place mostly at the front surface of the chip. The thermal diffusion length in Si (thermal diffusivity $\alpha_{Si} = 0.88\,cm^2/s$)[17] is $\mu = \left(\frac{\alpha}{\pi f}\right)^{1/2} = 750\,\mu m$ at f = 50 Hz. It means that a negligible amount of modulated heat reaches the PZT sensor in this case, thus excluding the pyroelectric contribution to the signal.

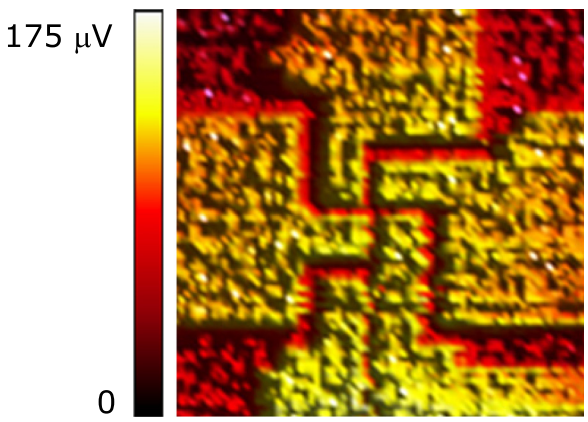

FIG. 2. PZT signal amplitude maps under modulated Ar^+ laser excitation. Scanned area: 200 μm × 200 μm.

The significant contribution comes from the piezoelectric effect produced by centimeter long wavelength acoustic waves that are generated by the laser absorption and subsequent heat production at the top surface of the sample. Here, the contrast displaying the tracks geometry (also observed in the phase map—not shown) expresses the optical absorption differences between the structures formed by polycrystalline silicon-SiO_2-Si substrate and by SiO_2-Si substrate. However, there are additional effects involved in the contrast definition: (i) the mismatch between the thermal properties of polycrystalline silicon and SiO_2 partially confines the heat produced inside the track, while outside heat propagates downward the substrate in an almost spherical way; (ii) acoustic waves produced in the tracks are subjected to reflections at the two interfaces of the silica layer. Actually, when the excitation laser strikes the track, the production of acoustic waves is hardly influenced by the mechanical bond of the whole structure, as well as by the local distinction between its mechanical properties.

Figure 3 presents results on the resistive polycrystalline silicon track biased with a modulated voltage at f = 25 kHz and with $V_0 = 4.0$ V. The scanned area (162 μm × 173 μm) covers the central part of the trail, as in the case of the measurement shown in Fig. 2. Voltage bias was applied in pads number 2, 3, and 4, while pad number 1 was kept grounded (see Fig. 1(b)). Figures 3(a) and 3(b) display the signal amplitude maps registered at the 2nd harmonic (2f) for PZT and the thermoreflectance detection, respectively.

In order to obtain the PZT image, a 488 nm non-modulated laser beam was used to scan the sample surface. As stated before, the addition of the non-modulated laser creates a supplementary modulated PZT signal component that discriminates the lateral regions of the sample. The image of Fig. 3(a) undoubtedly discloses the resistive tracks structure. The four branches carrying electric current (connected to pads number 1, 2, 3, and 4) are revealed both in amplitude (higher values on the track and nearby) and in phase (map not shown). Moreover, the bottom part of the central vertical line, which does not carry any electric current, is exhibited in the same way (with smaller amplitude). On the other hand, the metallic pads and the metallic track connected to pad number 3 do not evidence significant contrast.

Figure 3(b) must be used as a comparative reference to the PZT map, since the thermoreflectance signal is well established in operating microelectronic devices. It generally reveals the Joule heat dissipation feature of the circuit, being therefore, closely related to the electric current density distribution. The volumetric heat power density released by Joule effect in the track is given by

$$(\text{power/volume}) = (J^2/\sigma) = \sigma E^2 \qquad (1)$$

with σ being the electric conductivity, and J and E the magnitude of the electric current density and of the electric field, respectively. Therefore, the amount of heat released per unit time and per unit volume is proportional to the square of the applied voltage, V^2, and

$$V^2 = (V_0/2)^2\{1 + \cos(\omega t)\}^2 = V_0^2\{(3/8) + (1/2)\cos(\omega t) + (1/8)\cos(2\omega t)\}. \qquad (2)$$

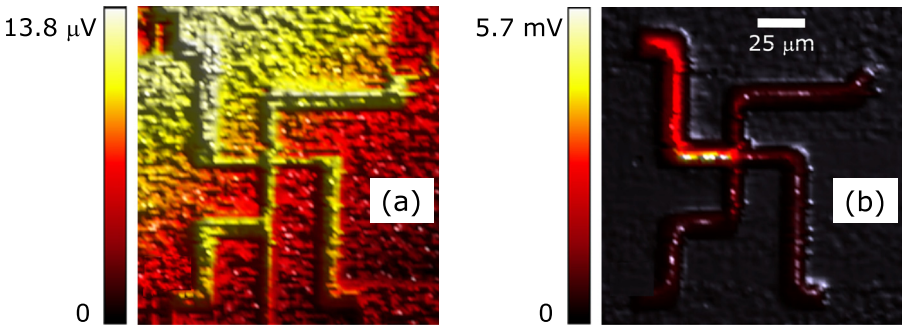

FIG. 3. (a) PZT and (b) thermoreflectance 2nd harmonic signal amplitude maps under modulated voltage excitation. Scanned area: 162 μm × 173 μm; modulated voltage: $V_0 = 4.0$ V, f = 25 kHz.

As one can see from Eq. (2), the Joule effect presents both the 1st and the 2nd harmonic. Indeed, the 2nd harmonic signal amplitude of the thermoreflectance, with the probe laser on the top of the biased track, follows clearly a V_0^2 curve (measurements not shown). Moreover, the local volumetric density of heat dissipation is proportional to the square of the magnitude of the current density (see Eq. (1)). This explains the maximum signal amplitude at the left side of the internal cross in Fig. 3(b), which is the narrowest one (6 μm wide) and carries the total electric current supplied by the function generator. Accordingly, smaller signal amplitude is observed at the portion of the track connected to pad number 1, since it is wider than the central part. The signal amplitude is strongly reduced in the other three branches of the internal cross because the electric current is split into the pathways. It is even smaller in the wider parts of the track connected to pads number 2, 3, and 4. Finally, it is easy to observe that the signal amplitude is quite small at the metallic track (signalized by the arrow in Fig. 1(b)), and at the pads themselves. This is explained taking into account the larger size of these structures and the higher thermal and electric conductivity/diffusivity of the metal compared with the polycrystalline silicon. Besides the smaller heat dissipation, the larger size of the tracks facilitates the heat spreading out from the source, thus reducing the local temperature variation.

Mismatch in the temperature coefficient of the reflectance, $(\frac{\partial R}{\partial T})$, and optothermal interference phenomena[13,15] are also involved in the response contrast between polycrystalline silicon, metal, and Si substrate regions. Indeed, the thermal diffusion length at 25 kHz is 34 μm in silicon and about 3 μm in the SiO_2 layer.[19] It means that the heat generated inside the track must spread out to Si substrate through the SiO_2 layer, although a significant heat confinement must occur due to thermal properties mismatch between polycrystalline silicon and silica. However, despite the existence of temperature modulation outside the track, the distinct thermo-optical response of the track itself makes the contrast observed in Fig. 3(b), as well as in other reported thermoreflectance measurements on biased tracks (see Ref. 15, for instance), exceptionally sharp.

Going back to the analysis of the PZT signal of Fig. 3(a), it is worth to say that, although the image reveals the tracks feature, the signal amplitude distribution does not match that of Fig. 3(b), i.e., the distribution of electric current supplied by the function generator. Actually, the bottom part of the central vertical line, represented by R_C in Fig. 1, is clearly visible in Fig. 3(a) and definitely does not carry any steady-state electric current. Even then, the PZT signal is still present both in the 1st and in the 2nd harmonics (the latter depicted in Fig. 3(a)). Furthermore, it scales as the second power of the voltage magnitude, as it can be seen from Fig. 4, which shows the PZT 2nd harmonic signal amplitude as a function of the square of the applied voltage V_0 at f = 25 kHz. In this figure, the data points represented by squares were obtained without the use of the laser beam (laser off). This contribution to the PZT signal comes from Joule effect produced in the whole circuit directly by the applied voltage, and constitutes the main part of the background signal of Fig. 3(a). The Joule dissipation at the resistive track at the top of the chip is detected by the PZT, which is located underneath the chip capsule. The thermal diffusion length of Si at 25 kHz is 34 μm, which strongly attenuates the thermal wave transmitted through the substrate and the backing of the chip capsule, until reaching the sensor. Again, the conclusion is that acoustic waves are the dominant mechanism to carry the information from the heat source to the PZT detector, the same as observed in Fig. 2. The triangles in Fig. 4 represent measurements made using the non-modulated (laser on), focused out of the tracks (on the substrate), in the central part of the circuit. Indeed, the measured signal at this condition is not dependent on the laser intensity. The dashed line in Fig. 4 is the linear best fit to these data (squares and triangles taken altogether), thus indicating their dependence with V_0^2.

The incremental signal that appears when the non-modulated laser strikes the sample becomes particularly significant nearby the resistive tracks. The circles in Fig. 4

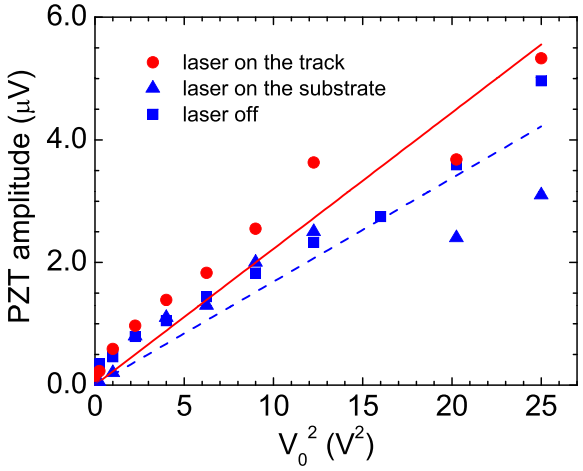

FIG. 4. PZT 2nd harmonic signal amplitude as a function of the square of the modulated applied voltage V_0.

represent the PZT 2nd harmonic signal amplitude as a function of the square of the applied voltage V_0, with the laser hitting the center of the track (under current flow). The solid line is the linear best fit to these data, indicating that the signal still has the quadratic dependence on the applied voltage (Joule effect). Using the fitted curves, it can be seen that the incremental signal is of the order of 30%. This additional contribution to the PZT signal exhibits the tracks conducting electric current, but also those parts without current flow. The contrast comes from the laser absorption in the track and in the close proximity to it. The absorbed light, both by the polycrystalline silicon track and by the silicon substrate in the vicinity of the track, gives rise to the production of local non-modulated heat and electron-hole pairs. The local modulated electric field along the track, which is responsible for the current flow at first, acts on these photo-injected electrons and holes, accelerating them and producing an additional carrier drift, which is in turn, modulated at the voltage frequency. This longitudinal modulated drift of photo-injected carriers would explain the supplementary signal all the way of the current flow. The hypothesis of photo-injected carrier modulation is supported by the fact that, on the metallic parts (track and contact pads), the additional contribution is absent.

In the case of the branches that do not carry electric current, such as the bottom part of the central vertical line in Fig. 3(a), there is no longitudinal component of the electric field (no longitudinal voltage gradient). However, once a uniform voltage is applied in a certain region of the resistive track, there appears a voltage gradient in the substrate, i.e., an electric field with components parallel and perpendicular to the resistive line, which in turn can modulate the photo-injected carriers at the very close vicinity of the track. In the case of the bottom part of the vertical line of Fig. 3(a), the applied voltage oscillates at the frequency f with intermediate amplitude, since it is connected to the central part of the resistive loop. The signal level that would come from this potential modulation is also intermediate, as observed from Fig. 3(a).

Finally, the background signal in Fig. 3(a), i.e., the signal recorded when the non-modulated laser impinges the Si substrate, far from the conducting tracks, also presents a specific aspect, i.e., it increases towards pad number 1 (the grounded pad). This fact is consistent with the expected distribution of the modulated electric field lines in the Si substrate under the applied bias: the lines originate in the tracks, which are at an elevated potential, and converge to the pad number 1 that is grounded, crossing the semiconductor substrate. Therefore, the concentration of lines is higher near the pad number 1, as it is the measured signal amplitude. It has to be mentioned that similar behavior was observed when acquiring the PZT signal amplitude map under distinct polarizations, namely, when connecting V_0 separately only to pad number 2 (or 3, or 4), or to pairs of pads as 2–3, 2–4, and 3–4, with pad number 1 grounded. In these cases, the overall signal intensity changes, as expected, and the background signal distribution is roughly maintained. As a final comment, focusing and defocusing of the laser spot when scanning the sample surface is completely excluded considering the measurements of Figs. 2 and 3(b).

Besides the Joule effect caused by the photo-injected carrier drift (along and perpendicular to the tracks), other possible mechanisms for the PZT signal associated with the non-modulated laser absorption are the carrier recombination, particularly at the materials interfaces, and the generation of acoustic waves by the electric field strength associated to the photo-injected carriers. Both mechanisms could be present, at the frequency f, in the regions where there is no net current flow in the track. On the other hand, artifacts such as the modulation of the laser absorption produced by the lateral displacement of the track edge (thermal expansion) are far below the noise level. Typical values of such displacement would range between 10^{-6} and 10^{-3} the size of the beam's spot. This would introduce a signal contribution of the order of 10^{-6}–10^{-3} the thermoacoustic signal amplitude of Fig. 2, i.e., a signal ranging in the pV-nV scale. The same applies to the normal (vertical) displacement of the track (change in its thickness). References 8, 13, and 15 report the detection of thermal displacement of sample features (diode laser length, coating layer thickness), using a reflected probe laser beam. Length changes of angstroms[8] and thickness variations of nanometers or less[13,15] were observed. However, the extremely high sensitivity in those cases is possible only because the probe beam intensity is modulated by knife edge and interference effects. Finally, one has to notice that the bottom of the central vertical line (characterized by R_C in Fig. 1) does not carry any current, being free of thermal expansion effects. Nonetheless, the thermoacoustic signal is clearly displaying the track feature.

In conclusion, a combined thermoacoustic and thermoreflectance set-up was presented and applied to the imaging of resistive tracks fabricated on a test chip. Two distinct excitation methods were used: the conventional modulated laser beam absorption and voltage/current modulation across the circuit. In the first case, the distinct materials structure is revealed through the PZT detection scheme, as expected. It is worth to emphasize the excellent sensitivity of the thermoacoustic detection, since the sensor is placed underneath the sample, what makes excitation point and sensor distanced by the whole substrate thickness and the chip capsule backing. The second excitation method (voltage/current modulation) exhibits the current flow through the thermoreflectance detection. In this very well established technique, the acquisition of a given point of the image is made by placing the probe beam at the desired position on the sample surface. This procedure pinpoints the signal source and allows the image construction. On the other hand, the thermoacoustic detection averages the signal coming from the entire sample. Furthermore, the method of excitation (voltage/current modulation) heats the whole circuit as well and no imaging emerges from this type of measurement. However, the addition of a focused non-modulated laser beam scanning the sample astonishingly showed to be useful in revealing the circuit track structure and the current and voltage distributions. The key of the proposed technique is the carrier photo-injection by the non-modulated laser beam. These carriers are, in turn, driven by the applied modulated electric field, thus resulting in heat and acoustic wave production at the located point of the laser absorption. This composed excitation method associated with the acoustic detection proved to

be sensitive to the voltage distribution, becoming a complementary technique to the well-established current flow map achieved through thermoreflectance measurements.

The authors acknowledge the Brazilian agencies FAPESP, CNPq, and FAEPEX-Unicamp, as well as CONACYT, México, for financial support. This work was supported by research Grant Nos. SIP-IPN-20150390, 20160144, and CONACyT-2011-01-174247. The support of COFAA-IPN through the SIBE and BEIFI Programs is also greatly acknowledged.

[1]A. Rosencwaig, J. Opsal, W. L. Smith, and D. L. Willenborg, Appl. Phys. Lett. **46**(11), 1013–1015 (1985).
[2]A. M. Mansanares, T. Velinov, Z. Bozoki, D. Fournier, and A. C. Boccara, J. Appl. Phys. **75**(7), 3344–3350 (1994).
[3]L. Pottier, Appl. Phys. Lett. **64**(13), 1618–1619 (1994).
[4]F. Lepoutre, D. Balageas, Ph. Forge, S. Hirschi, J. L. Joulaud, D. Rochais, and F. C. Chen, J. Appl. Phys. **78**(4), 2208–2223 (1995).
[5]L. R. de Freitas, A. M. Mansanares, and E. C. da Silva, Rev. Sci. Instrum. **74**(1), 735–737 (2003).
[6]P. W. Epperlein, Jpn. J. Appl. Phys. **32**, 5514–5522 (1993).
[7]A. M. Mansanares, D. Fournier, and A. C. Boccara, Electron. Lett. **29**(23), 2045–2047 (1993).
[8]A. M. Mansanares, J. P. Roger, D. Fournier, and A. C. Boccara, Appl. Phys. Lett. **64**(1), 4–6 (1994).
[9]L. C. O. Dacal, A. M. Mansanares, and E. C. da Silva, J. Appl. Phys. **84**(7), 3491–3499 (1998).
[10]A. Mandelis, A. Williams, and E. K. M. Siu, J. Appl. Phys. **63**(1), 92–98 (1988).
[11]J. A. Batista, A. M. Mansanares, E. C. da Silva, and D. Fournier, J. Appl. Phys. **82**(1), 423–426 (1997).
[12]B. C. Forget, S. Grauby, D. Founier, P. Gleyzes, and A. C. Boccara, Electron. Lett. **33**(20), 1688–1689 (1997).
[13]J. A. Batista, A. M. Mansanares, E. C. da Silva, C. C. Vaz, and L. C. M. Miranda, J. Appl. Phys. **88**(9), 5079–5086 (2000).
[14]L. R. de Freitas, E. C. da Silva, A. M. Mansanares, M. B. C. Pimentel, S. Eleutério Filho, and J. A. Batista, J. Appl. Phys. **97**, 104510 (2005).
[15]L. R. de Freitas, E. C. da Silva, A. M. Mansanares, G. Tessier, and D. Fournier, J. Appl. Phys. **98**, 063508 (2005).
[16]S. Galovic, Z. Soskic, and D. M. Todorovic, in *Microscopy: Science, Technology, Applications and Education*, edited by A. Méndez-Vilas and J. Díaz (Formatex Research Centre, Spain, 2010), pp. 1506–1515.
[17]E. Marin, E. Hernández-Rosales, A. M. Mansanares, R. Ivanov, J. B. Rojas-Trigos, and A. Calderón, Rev. Sci. Instrum. **84**, 104903 (2013).
[18]J. B. Rojas-Trigos, E. Marin, A. M. Mansanares, E. Cedeño, G. Juarez-Gracia, and A. Calderon, Thermochim. Acta **582**, 101–105 (2014).
[19]A. M. Mansanares, M. L. Baesso, E. C. da Silva, F. C. G. Gandra, H. Vargas, and L. C. M. Miranda, Phys. Rev. B **40**, 7912–7915 (1989).